Biomedical Physics &
Engineering Express

Endorsed by IPEM Institute of Physics and Engineering in Medicine

PURPOSE-LED PUBLISHING™

PAPER • OPEN ACCESS

Supercapacitor-based pulse generator with waveform adjustment capability for small animal transcranial magnetic stimulation

To cite this article: Soniya Raju *et al* 2025 *Biomed. Phys. Eng. Express* **11** 015045

IOP Publishing Biomed. Phys. Eng. Express 11 (2025) 015045 https://doi.org/10.1088/2057-1976/ad9f6b

Biomedical Physics & Engineering Express

OPEN ACCESS

RECEIVED
12 September 2024

REVISED
9 December 2024

ACCEPTED FOR PUBLICATION
16 December 2024

PUBLISHED
26 December 2024

PAPER

Supercapacitor-based pulse generator with waveform adjustment capability for small animal transcranial magnetic stimulation

Soniya Raju[1], **Nihal Kularatna**[2], **Marcus Wilson**[1] **and D Alistair Steyn-Ross**[2]

[1] Te Aka Mātuatua School of Science, University of Waikato, New Zealand
[2] Te Kura Mata-Ao School of Engineering, University of Waikato, New Zealand

E-mail: sr231@students.waikato.ac.nz **and** marcus.wilson@waikato.ac.nz

Keywords: transcranial magnetic stimulation, Pulse circuits, supercapacitor, pulse shaping

Abstract

In transcranial magnetic stimulation (TMS), pulsed magnetic fields are applied to the brain, typically requiring high-power stimulators with high voltages and low series impedance. TMS pulse generators for small animal coils, are underexplored, with limited dedicated circuits and simulation models. Here, we present a new design for a high-power TMS pulse generator for small animals, utilizing a pre-charged supercapacitor that is sufficient to produce repeated pulses for TMS applications without the need for recharging. This approach eliminates the need for expensive high-voltage components and a high-voltage power supply. In this paper, we detail the design approach and basic block diagrams of a supercapacitor (SC) based TMS pulse generator, along with its experimental results. The findings indicate that the new circuit enables a complete test using just a single charge of an SC module. The proposed circuit functions as a versatile pulse-shaping device, where the MOSFET is treated as a dynamically varying resistor element rather than a traditional switch; allowing pulse parameter variations. We analyze a novel circuit for generating and controlling TMS pulses in small animal coils, and demonstrate its effectiveness through experimental results.

1. Introduction

Transcranial magnetic stimulation (TMS) is a non-invasive technique that uses electromagnetic induction to electrically stimulate neural tissue, including the cerebral cortex and peripheral nerves. Developed in the mid-1980s by Barker and colleagues (Barker *et al* 1985, 1991), TMS has become an essential tool in both experimental neuroscience and clinical practice (Wassermann and Zimmerman, 2012; Valchev et al 2018; Peterchev *et al* 2015). By modulating neuronal activity, TMS provides valuable insights into brain function and offers therapeutic benefits for various neurological and psychiatric disorders, including major depressive disorder, Parkinson's disease, stroke, and anxiety disorders (Iglesias 2020; Somaa 2022; George *et al* 2010; Menzies *et al* 2008; Osuch *et al* 2009; Camera *et al* 2024; Smith and Stinea 2016). TMS works by placing a stimulation coil over the head to generate rapidly changing magnetic fields. These pulses penetrate the scalp and skull, inducing secondary ionic currents in the brain tissue. Unlike direct electrical stimulation, which requires electrodes on the scalp, TMS induces currents non-invasively, offering high spatial and temporal precision (Gomez-Tames *et al* 2020).

High-voltage and high-power pulse generators are used in many applications such as transcranial magnetic stimulation (TMS), lightning surge simulators and fence energizers (Peterchev *et al* 2007). Typically these pulse generators are designed by combining a high-voltage DC source with pulse-shaping circuits and high-voltage semi-conductor switches (Mankowski and Kristianse 2000; Elserougi *et al* 2016; Zan *et al* 2023). Given the requirement for safety-related isolation within the circuits and the high cost of high-voltage components, the development of a high-power pulse generator poses significant challenges. Most human TMS pulse generators (Goetz *et al* 2012; Peterchev *et al* 2007; Koponen and Peterche 2020) are based on inverter topologies to generate a high-voltage pulse. Due to the constrained affordability of commercial pulse generators, research groups are motivated to develop their own high-power pulse generators (Selvaraj *et al* 2018; Peterchev and Murph 2013; Sorkhabi *et al* 2021; Ali *et al* 2023).

There are various approaches to designing and building high-power pulse generators in other applications as well (Yan *et al* 2020; Cheng *et al* 2021; Li *et al* 2015; Jiang *et al* 2022; Elgenedy *et al* 2017). Some start with a high voltage DC power supply followed by wave-shaping circuits (Peterchev and Murph 2013). Marx type pulse generators use voltage multiplier techniques (Cheng et al 2022). Similar to the Marx generator, a Tesla transformer is also used to charge a pulse forming circuit (Zhao et al 2019). Despite innovations like solid-state Marx generators and Tesla transformers aimed at enhancing efficiency, these systems remain complex, expensive, and require multiple stages and components.

Moreover human TMS topologies are unsuitable for small-animal stimulation coils for several reasons. Firstly, constructing a medium to high voltage circuit for such a small coil is challenging. Additionally, it is crucial to address heating and losses associated with the small animal coil and ensure adequate protection. The literature provides mouse-specific TMS circuits designed to address these challenges (Wilson et al 2018; Tang et al 2017; Selvaraj et al 2018; Nieminen et al 2022; Khokhar et al 2021; Tang et al 2016). These circuits are tailored to accommodate the smaller size of the coil, provide appropriate voltage levels for stimulation, and mitigate heating and losses associated with the smaller coil size. Additionally, TMS pulse generators, especially those for small animals, are under-explored, with limited dedicated circuits and simulation models. A supercapacitor-based pulse generator (Raju et al 2023) offers a promising solution, leveraging higher energy density, rapid charging and discharging capabilities, and longer lifetimes. The supercapacitor approach could provide efficient, cost-effective, TMS pulse generation for small animals.

Most small animal brain stimulation research (Selvaraj et al 2018; Khokhar et al 2021; Nieminen et al 2022) has relied on common circuits rather than specifically designed ones. These circuits typically use capacitor discharging and free-wheeling through diodes or inverter topologies. A significant drawback is the lack of a specific input source, necessitating either a high-voltage supply or a high-voltage capacitor, depending on the application, or a basic DC lab supply for smaller circuits. The primary differences among these circuits are found in the driving circuitry or control mechanisms, and they often lack provisions for pulse shaping.

Here, we describe the development of a pulse generator prototype for small animal TMS coils (Wilson et al 2018; Khokhar et al 2021; Tang et al 2015, 2018). A new supercapacitor-based pulse generator approach for TMS (Raju et al 2023) draws from research on supercapacitor use in power converters and protection systems (Kularatna and Jayanand 2020; Udayanga et al 2021). This design leverages the energy storage capabilities of supercapacitors to deliver consistent and reliable pulses for TMS without the need for traditional high-voltage components.

This article details our research on developing an electronic circuit for TMS pulse shaping. There are currently very few dedicated circuits (Tang et al 2016; Khokhar et al 2021) designed specifically for mouse coils, and the ones that exist offer limited pulse-shaping capabilities. Addressing this gap in the literature, we have developed a novel prototype circuit with wave-shaping functionality and a self-sufficient power source capable of producing continuous TMS pulses. Traditional TMS circuits typically employ MOSFETs as simple switches (Peterchev et al 2007; Goetz et al 2012; Sorkhabi et al 2021). However, MOSFETs can also be utilized to achieve finer control over coil current and voltage. This study introduces an innovative pulse-shaping method that involves dynamically varying the gate voltages of MOSFETs, enabling them to act as dynamic elements rather than only switches. This approach significantly enhances TMS pulse-shaping capabilities without requiring substantial additional hardware.

2. Adequacy of a low-cost SC module as the primary energy source for a TMS pulse generation

2.1. General properties of commercial SC compared to electrolytic capacitors

Within the past decade, supercapacitors (SCs) have rapidly developed as a long-life energy storage solution. Technically, an SC can be considered to have a capacitance that is one million times larger than that of a typical electrolytic or film capacitor of the same canister size.

Compared to a rechargeable battery, an SC is capable of delivering very high power due to its extremely low equivalent series resistance (ESR). When a capacitor is connected to a load the maximum power delivery is governed by the internal resistance of the capacitor. The power transfer theorem (Kularatna and Gunawardan 2021) predicts that the maximum power deliverable by the capacitor is

$$P_{\max} = \frac{V_{oc}^2}{4r_c} \tag{1}$$

However, the primary limitation of an SC is its low DC rating compared to an electrolytic capacitor. Table 1 compares the key specifications of these two device families from a designer's perspective.

2.2. Power and energy delivery capabilities of supercapacitors and normal capacitors

Supercapacitors are designated as high power-density devices owing to their remarkably low ESR, typically 1 to 2 orders of magnitude smaller than that of electrolytic capacitors. Table 1 compares power delivery capability and maximum energy content for a representative set of paired supercapacitors and electrolytic capacitors having similar canister volumes.

Supercapacitors have medium energy density with high-power density (calculated by $\frac{V_{oc}^2}{4r_c}$ /mass). A similarly-sized electrolytic capacitor has higher power delivery capability but lower energy storage capacity.

Table 1. comparison of the supercapacitors and electrolytic capacitors.

Capacitor (F)	Rated voltage (V)	ESR (mΩ)	Max current[a] (A)	Short circuit current[b] (A)	Max power[c] (W)	Max energy (J)
25	3	30	21	100	75	112.5
100	3	8	78	375	281	450
[d]**380**	**3**	**3.2**	**250**	**937.5**	**70**	**1800**
500	3	3.2	288	937.5	703	2250
3000	3	0.23	2663	13 k	9.7 k	13.5 k
220 μ	450	1206	2.34	0.37 k	42 k	22.3
[d]**330** μ	**450**	**340**	**3.62**	**1.3 k**	**148.9 k**	**33.4**
680 μ	200	36	4.15	5.5k	277.7 k	13.6
2200 μ	400	60	16	6.7 k	666.7 k	176
5600 μ	500	49	21	10.2 k	1275 k	700

[a] continuous rated current given by the data sheet.
[b] estimated instantaneous short-circuit current V_{oc}/r_c.
[c] maximum instantaneous power.
[d] highlighted rows correspond to the capacitors used in the TMS stimulation circuit described in this manuscript.

Electrolytic capacitors are unable to sustain high power delivery over an extended period due to their low time constant.

2.3. Concept behind the SC-based TMS pulse generator

As shown in table 1, a SC can store enough energy to generate a series of TMS pulses, based on its energy storage capacity, as listed under the maximum energy column. For example, a 95 F SC can store approximately 45 J with 1 V voltage, which is sufficient to generate over 190 TMS pulses. If we use a 3000 F SC, the number of pulses would significantly increase to 2000. This energy storage capacity can be further increased by charging the supercapacitor to a higher voltage, allowing it to store even more energy and thereby generate a greater number of TMS pulses. However, given that SCs typically have a low rated voltage, a voltage step-up circuit is necessary to raise the voltage to the required level for stimulation.

In Khokhar *et al* (2021), a DC supply with an output impedance of 10 Ω was used, while Tang *et al* (2016) employed a bipolar voltage-programmable power supply (KEPCO BOP 100-4M, TMG Test Equipment, Melbourne, Australia) with an output impedance of 4 mΩ. In comparison, using a supercapacitor results in significantly lower equivalent series resistance (ESR), with values as low as 0.23 mΩ as the capacitance increases (see table 1).

In section 3, we demonstrate how a supercapacitor-based primary energy source can be connected to an electrolytic capacitor-based output stage using inexpensive magnetic components and solid-state switches.

3. Prototype construction

Figure 1 depicts the overall block diagram of this supercapacitor-based high-power pulse generator. In the block diagram representation, there are two stages highlighted by red and blue dotted rectangles. The first stage (red dashed block) is the power stage, which handles high voltage and current. The second stage (blue dashed block) is the switching control stage, which operates at low voltage. An opto-isolator is used to isolate these two stages, ensuring electrical protection and safety. Since this research focuses solely on the development of the electronic circuit, without involving any animal testing, only circuit protection measures have been implemented.

3.1. Charging circuit (Block 1)

For this prototype, the supercapacitor bank is charged to 5 V using a standard 3 A, 0–30 V laboratory DC power supply (BK precision 1670A). This block can be disconnected once the supercapacitor module has reached the required voltage level, as the supercapacitor is capable of producing pulses without the need for recharging.

3.2. Pre-storage primary energy source (Block 2)

The Block 2 (figure 1) primary energy source is a supercapacitor bank (C_1) constructed from four 3-V, 380-F supercapacitors connected in series to give a net capacitance of 95 F, and a maximum working voltage of 12 V.

It can produce up to 6840 pulses with a 12 V input with each pulses of 2 J of energy and a voltage drop of only 0.2 V per discharge in the supercapacitors. Utilizing a higher capacity supercapacitor (SC) could produce significantly more pulses with an even smaller voltage drop ($\approx$ 0.02 V with a 3000 F SC). With larger capacitance, the energy density is also higher, allowing the supercapacitor to sustain a greater number of pulses with a single charge. Figure 2 presents the experimental results obtained using the prototype with a 1 V supply, demonstrating pulse count capacity across supercapacitors with different capacitance values.

One key advantage of this design is that the series-connected SC module can be pre-charged by any suitable laboratory power supply and the SC module can

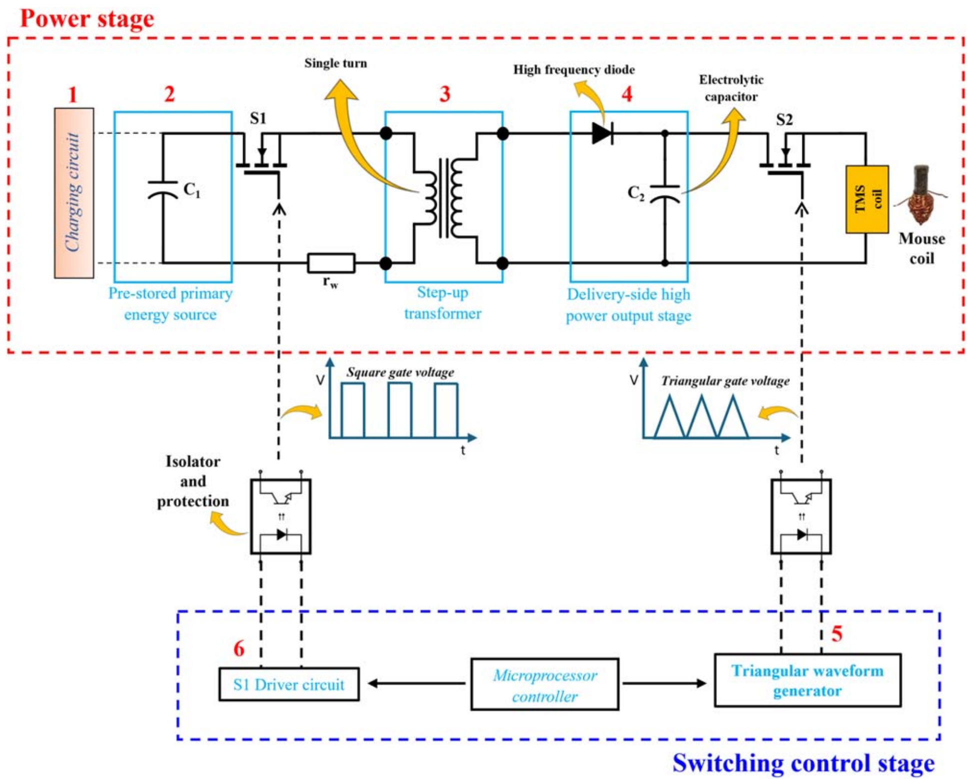

Figure 1. Block diagram of prototype TMS pulse generator. Power stage (high voltage) and switching control stage (low voltage) highlighted by red and blue dotted rectangles respectively. An opto-isolator isolates the stages for protection and safety.

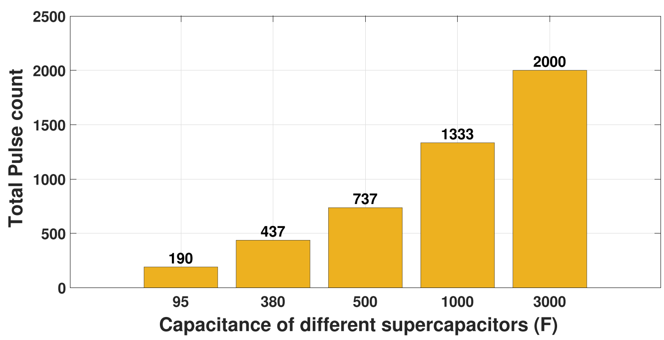

Figure 2. The total TMS pulse generated using the prototype with a 1 V input and tested with supercapacitors of varying capacitances. Pulses of 100 μs duration with a 200 V (1st pulse) amplitude were observed.

be used for repeated sets of pulses for a given experiment without the need for the DC power supply to be connected continuously.

3.3. Step up transformer (Block 3)

Given that a TMS coil requires an excitation voltage of several hundred volts, we must increase the output voltage of the supercapacitor bank by a significant factor. For this purpose, we have tested the suitability of a step-up transformer with a single-turn primary and large turn ratio (1:60 range). The single-turn primary allows a high drive current into the transformer's primary winding. The equivalent circuit of a transformer, as discussed in Valchev and den Bossch (2018), is shown in figure 3. Referring to figure 1 and figure 3, and symbol definitions in table 2, the initial voltages appearing across the primary and secondary coils are:

$$v_p = V_{oc} - (r_c + r_w + r_p)i_p \quad (2)$$

$$v_s = n \quad v_p \quad (3)$$

where $n = N_s/N_p$ and V_{oc} is the open-circuit voltage of the supercapacitor bank. If the parasitic resistances r_c, r_w (wire resistance) and r_p are too large, the primary voltage will be too low to create a high-power output pulse.

As per the definition of self-inductance (Valchev and den Bossch 2018), the total self-inductance of primary (L_1) and secondary (L_2) windings can be expressed as the sum of magnetizing and leakage

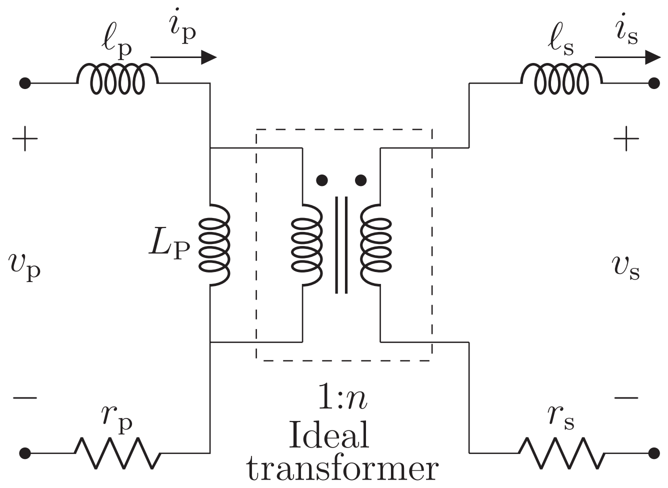

Figure 3. Equivalent circuit of the transformer.

Table 2. Symbol definitions and values for the transformer equivalent circuit.

Symbol	Description	Measured values primary, secondary
L_p, L_s	Magnetizing inductance for primary, secondary	8.33 μH, 32.5 mH
ℓ_p, ℓ_s	Leakage inductances	0.29 μH, 977 μH
r_p, r_s	Winding resistance	5.8 mΩ, 12 Ω
N_p, N_s	Number of turns	1, 60
v_p, v_s	Transformer voltages	–
i_p, i_s	Transformer currents	–

components:

$$L_1 = L_p + \ell_p, \tag{4}$$

and

$$L_2 = L_s + \ell_s. \tag{5}$$

By referring all inductive components to the secondary, the total self-inductance of the secondary side is:

$$L_2 = n^2(L_p + \ell_p) + \ell_s. \tag{6}$$

Inductance for both windings was measured using a Fluke PM6304 LCR meter at 10 kHz; see table 2. From equation (6), the secondary winding will have a total self-inductance of $L_2 = 32$mH, thus the secondary circuit is highly inductive. In this preliminary design the transformer was wound on a highly-permeable toroidal ferrite core type ZW42207TC (Magnetics) using a turns ratio of 1:60.

3.4. Delivery-side high-power output stage (Block 4)

A high-frequency diode and a high-voltage rated electrolytic capacitor (C_2) are coupled to the secondary of the transformer to achieve a DC output voltage which is sufficient to drive a high-power pulse into the TMS coil. Given that the transformer secondary has a high inductance which comes in series with the diode and capacitor in the secondary side, during each 'on' period of Switch-1 (MOSFET S1 in figure 1) there will be limited charge accumulation in the electrolytic capacitor. In order to charge the capacitor to the required voltage it is necessary to repetitively trigger S1. So the processor (Block 6) drives the gate of S1 with a pulse repetition rate of 8 kHz for a total integration time of 2 s. During this charging time, MOSFET S2 is 'off'. The energy stored in the electrolytic capacitor is then delivered to the TMS coil by driving the output MOSFET (S2 in figure 1) with a triangular gate-control voltage (Block 5). A full circuit diagram is shown in figure 4. The analysis of a resistor-diode combination placed in parallel with the TMS coil is explained in section 6.

The TMS coil is modeled as an inductance L in series with an internal resistance r_L (see figure 5). The coil is energized by discharging the electrolytic capacitor (C_2) via the non-linear resistance r_{DS} of MOSFET S2. The time-varying current i_L is measured with a current-clamp probe (Tektronix A622), then validated with MATLAB by integrating the measured inductor voltage $v_L{}^{meas}$. Figure 6 shows (a) the gate voltage, (b) the voltage over the C_2 and the current through the coil, and (c) the voltage over the coil and the drain-source voltage, as a function of time. We first identify from figure 6 the voltage over the coil (without resistance) as:

$$v_L(t) = L\frac{di_L}{dt} = v_L{}^{meas}(t) - i_L(t)r_L \tag{7}$$

We map this first-order differential equation to a finite difference equation approximation by mapping $di_L \rightarrow \Delta i_L = (i_L{}^{n+1} - i_L{}^n)$, and $dt \rightarrow \Delta t$, the oscilloscope time base resolution (time between consecutive samples). This

$$L\frac{i_L{}^{n+1} - i_L{}^n}{\Delta t} = (v_L{}^{meas})^n - i_L{}^n r_L \tag{8}$$

giving an Euler update equation for $i_L{}^{n+1}$,

$$i_L{}^{n+1} = i_L{}^n + \frac{\Delta t}{L}((v_L{}^{meas})^n - i_L{}^n r_L) \tag{9}$$

where $n = 1\ldots N$ is the time-step index for a total of $N = 2500$ samples. The initial condition is

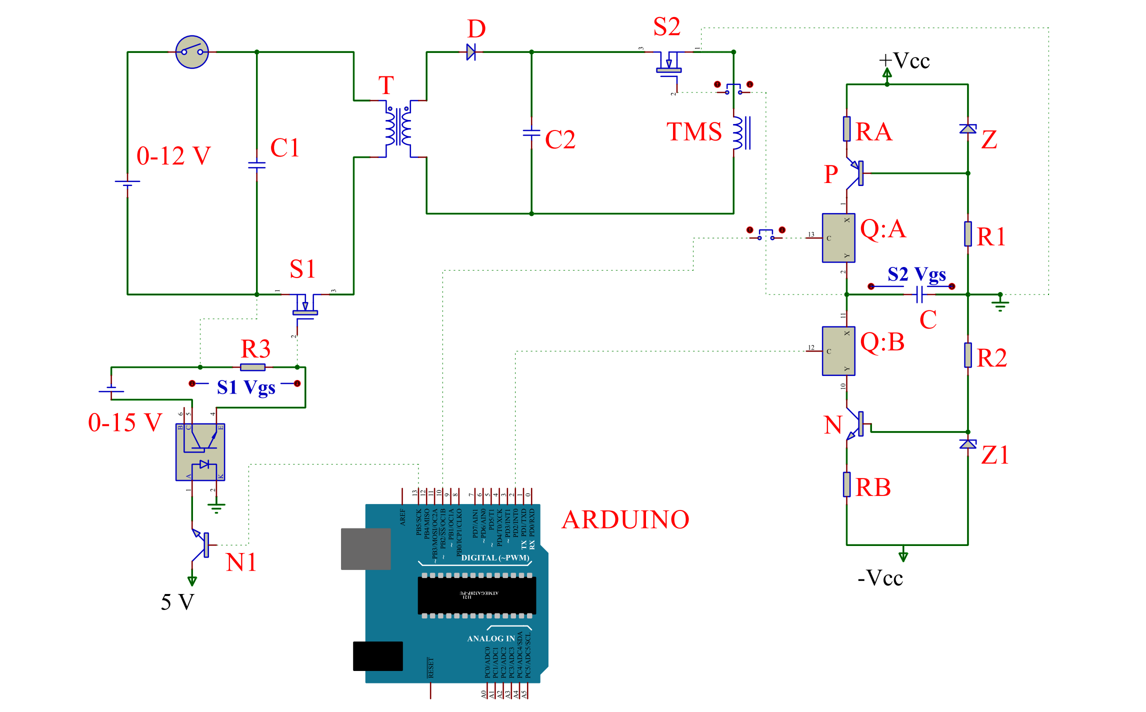

Figure 4. Circuit topology of the prototype.

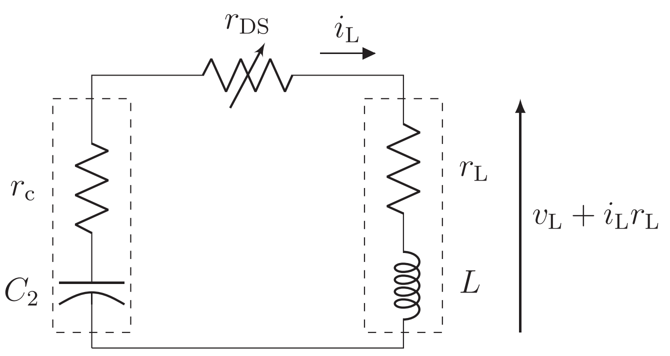

Figure 5. Equivalent model of the RLC circuit in the prototype consisting of the electrolytic capacitor C_2 with internal resistance r_{C}, non-linear resistance r_{DS} of MOSFET S2, and TMS coil with inductance L with internal resistance r_{L}.

$i_{\mathrm{L}}(t = 0) = 0 \rightarrow i_{\mathrm{L}}{}^{n=1} = 0$. We can thus predict the current at the $(n + 1)^{th}$ step given a measurement of coil voltage and current at the n^{th} step.

The comparison between modelled and measured currents is shown in figure 6. The current-probe has a bandwidth of dc-100 kHz, so gives a much slower response than the $v_{\mathrm{L}}{}^{\mathrm{meas}}(t)$ oscilloscope reading (bandwidth 0-10 MHz). To correct for current probe delay, we advanced the measured current trace by 2 μs prior to plotting (figure 6). This leftwards timing offset was also applied to the current traces displayed in MATLAB plots of figure 6, figure 7, figure 8, and figure 9.

3.5. Other requirements

There was no need for AC decoupling capacitors in the supply lines, as the circuit operates exclusively on DC power. The supercapacitors are charged using a DC power supply, and all wire lengths in the circuit have been kept as short as possible. Our goal was to design a low-cost and reliable pulse generator. To achieve this, we employed an optocoupler (figure 1), which performed exceptionally well. The optocoupler provided the correct gate voltage while ensuring effective isolation, thereby eliminating the need for a biasing resistor.

4. Circuit testing

In this proof-of-concept experiment, the S1 driver circuit with microprocessor block (Block 6 in figure 1) generates an 8 kHz square-wave voltage to repetitively trigger S1 until the output electrolytic capacitor (C_2) attains a predetermined voltage set at 30 V for this experiment. The gate voltage to S2 is provided by an adjustable triangular generator creating a triangular voltage waveform of variable slope.

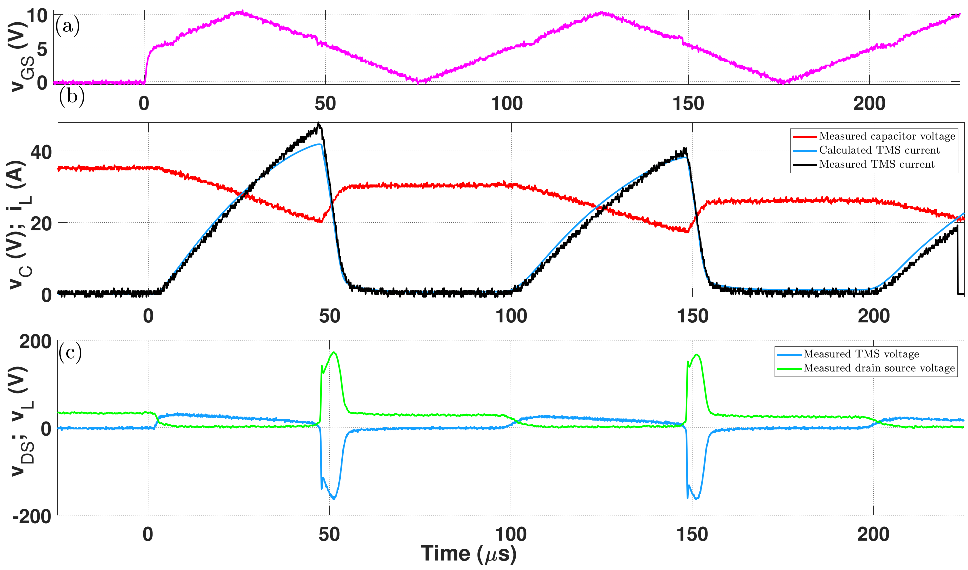

Figure 6. Circuit response measured during TMS coil excitation obtained with 1 V of input to the supercapacitor (a) Triangular control voltage of MOSFET 2 gate (the triangular wave is not captured for the initial 25 μs due to configuration of the triggering mechanism in the oscilloscope); (b) Measured electrolytic capacitor voltage (red) and measured/calculated TMS coil current (black/blue); (c) Drain-source voltage of MOSFET (green) and measured TMS coil voltage (blue).

In this study, the TMS coil constructed by Khokhar *et al* (2021) was utilized. As an initial phase, resistance and inductance measurements of the coil were conducted. The coil comprises 50 turns of copper wire with a conductive diameter of 0.4 mm wound around a 5 mm diameter carbonyl powdered iron core (Micro Metals, U.S.A). The inductance of the coil was measured to be 23 μH and resistance as 212 mΩ using an Agilent E4980A four-point impedance meter.

As shown in figure 6, the electrolytic capacitor (C_2) has a starting voltage of 30 V. This C_2 starting voltage was obtained by energy transfer (at 8 kHz for 2 s) from the C_1 supercapacitor that had been precharged to 1 V. C_2 is subsequently progressively discharged to the TMS coil by periodically triggering S2 with a 10 kHz triangular gate voltage with 50% symmetry (meaning the rise time is 50% of the total rise and fall time), generating a TMS pulse with a peak voltage 150 V, peak current 40 A, and peak instantaneous power 6 kW. The peak voltage is the inductive response to the rapid reduction in current when MOSFET S2 switches off.

We then increased the supercapacitor voltage to 3 V and activated S1 for a duration of 4 s, allowing the electrolytic capacitor to reach 100 V. Employing the same 50% symmetry and 10 V peak-to-peak triangular waveform to activate S2, we observed a TMS pulse with a peak negative voltage of amplitude 276 V, peak current 124 A, and a peak instantaneous power 34.2 kW. Results are shown in figure 7.

As illustrated in figure 8, by altering the symmetry of the 10 kHz triangular voltage drive to MOSFET S2, the circuit can generate significantly higher output voltages without re-configuring the hardware. Testing the configuration with 80% (80:20 rise-fall) symmetry resulted in a voltage pulse of amplitude 508 V. As well as amplitude, the system enables convenient adjustment of TMS pulse shape, including rise and fall time. A pronounced increase in peak coil voltage and the emergence of oscillations around 1 MHz, caused by fast switching transitions (dv/dt and di/dt) as well as parasitic inductance and capacitance, are observed in figure 8. This behaviour results from rapid turn-off and can be mitigated using an RC circuit in the TMS output stage and an improved gate driver circuit to mitigate the gate capacitance. Further investigation is required to fully understand and address this problem.

In addition, modification of gate-voltage amplitude allows further changes in the TMS current and voltage pulse characteristics. Figure 9(a) depicts the impact of varying the gate-voltage amplitude on the rise, fall, and pulse width of the TMS current waveform. Increasing the peak gate voltage from 7 V to 10 V increases the pulse width and pulse height of the TMS coil current. Figure 9(d) shows how the symmetry of the gate voltage influences the TMS voltage and current pulse shape, as well as the pulse width. A shorter fall time results in a shorter pulse duration but produces higher amplitude voltage pulses.

5. Magnetic field measurement

To measure the magnetic field produced, the coil was placed in an adjustable holder above a Hall effect sensor, figure 10(a). Existing literature (Tang *et al* 2016; Wilson *et al* 2018) indicates that magnetic field strengths of less than 200 mT are typically achieved for mouse coils. However, magnetic fields as high as 800 mT with a 50 V input have also been reported (Khokhar *et al* 2021), accompanied by an electric field

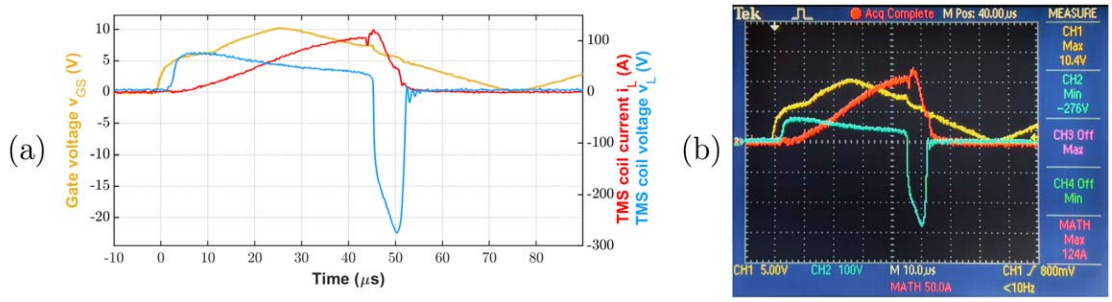

Figure 7. (a) Gate voltage, TMS coil current and TMS coil voltage against time. The raw traces captured from the oscilloscope (b) have been smoothed with a Whittaker filter (Weinert, 2007; Eilers, 2003) to reduce oscilloscope 8-bit digitization noise; (b) Oscilloscope measurement of MOSFET gate voltage (yellow), TMS coil voltage (blue) and TMS coil current (red). Symmetry is set at 50% with with a 3 V input in the supercapacitor bank.

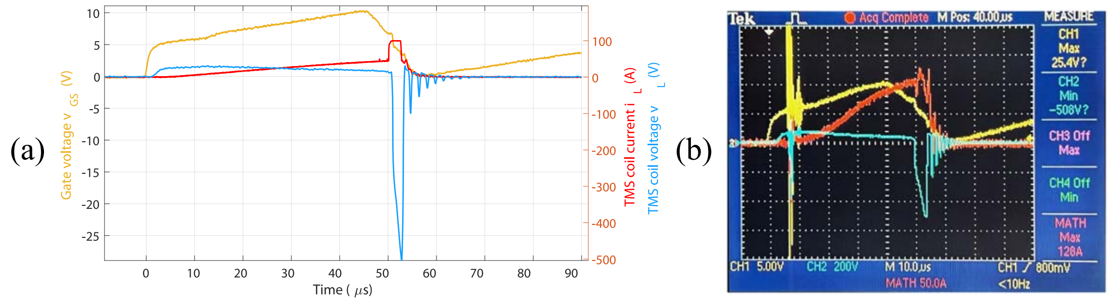

Figure 8. Gate voltage (yellow), TMS coil voltage (blue), and TMS current (red) for gate voltage symmetry at 80%. (a) MATLAB capture of oscilloscope traces of gate, voltage and current smoothed with a Whittaker filter; (b) Oscilloscope measurement. Note pronounced increase in peak coil voltage and emergence of $\approx$ 1 MHz oscillations arising from reduced gate-voltage fall time.

intensity of 10 V/m. However, with 80% symmetry and only with 1 V input from the supercapacitor, we were able to generate a magnetic field exceeding 200 mT, which may be sufficient to stimulate brain cells in small animals (Selvaraj *et al* 2018; Khokhar *et al* 2021). The magnetic field (B-field) measurement process utilized an SS496A1 Hall effect sensor. The Hall effect sensor was calibrated using a Helmholtz coil (Khokhar *et al* 2021). Figure 10(b) illustrate the magnetic flux density (B-field) from 0 mm to 4 mm distance from the coil with 80% symmetry gate voltage input.

For the 0 mm and 1 mm cases, the magnetic field exceeded the sensor's maximum range of 200 mT. To estimate the magnetic field beyond this range, a scaling factor was applied to the 2 mm results, ensuring that the estimated field aligns with the measured field below 200 mT (Khokhar *et al* 2021). Increasing the input voltage would enhance the output voltage and magnetic field strength. Higher input voltages would lead to increased C_2 voltage, resulting in higher induced voltages across the inductor and stronger magnetic fields.

6. Enhanced pulse shaping with resistor-diode combinations

Most TMS circuits incorporate a discharge path into the TMS coil circuit. This is often for the purpose of preventing high voltages over the switches, but also has the advantages that, the circuit gains additional control over the energy release from the coil, allowing for more precise manipulation of the pulse characteristics, such as width, amplitude, and overall shape.

The addition of a resistor-diode combination in parallel with the TMS coil (figure 11) serves a role in controlling the discharge rate of the coil when the MOSFET (S2) is turned off. This setup functions similarly to a snubber circuit, which is commonly used in electronic circuits to protect components and shape waveforms by controlling the voltage and current transitions.

When the switch S2 is on, the current flows through the TMS coil, storing energy in the magnetic field of the inductor. Without the R-diode (figure 4), upon turning off the switch S2, the current flow through the coil would typically drop rapidly leading to a high, potentially damaging voltage over S2. However the diode parallel to TMS coil (figure 11) allows the current to continue flowing through the resistor, rather than abruptly stopping. This creates a path for the inductor's stored energy to discharge more gradually. The resistor in the combination sets the rate at which the energy is dissipated. A higher resistance shortens the time it takes for the current to decay to zero, manifested through the $\frac{L}{R}$ time constant. Conversely, a lower resistance results in a more prolonged

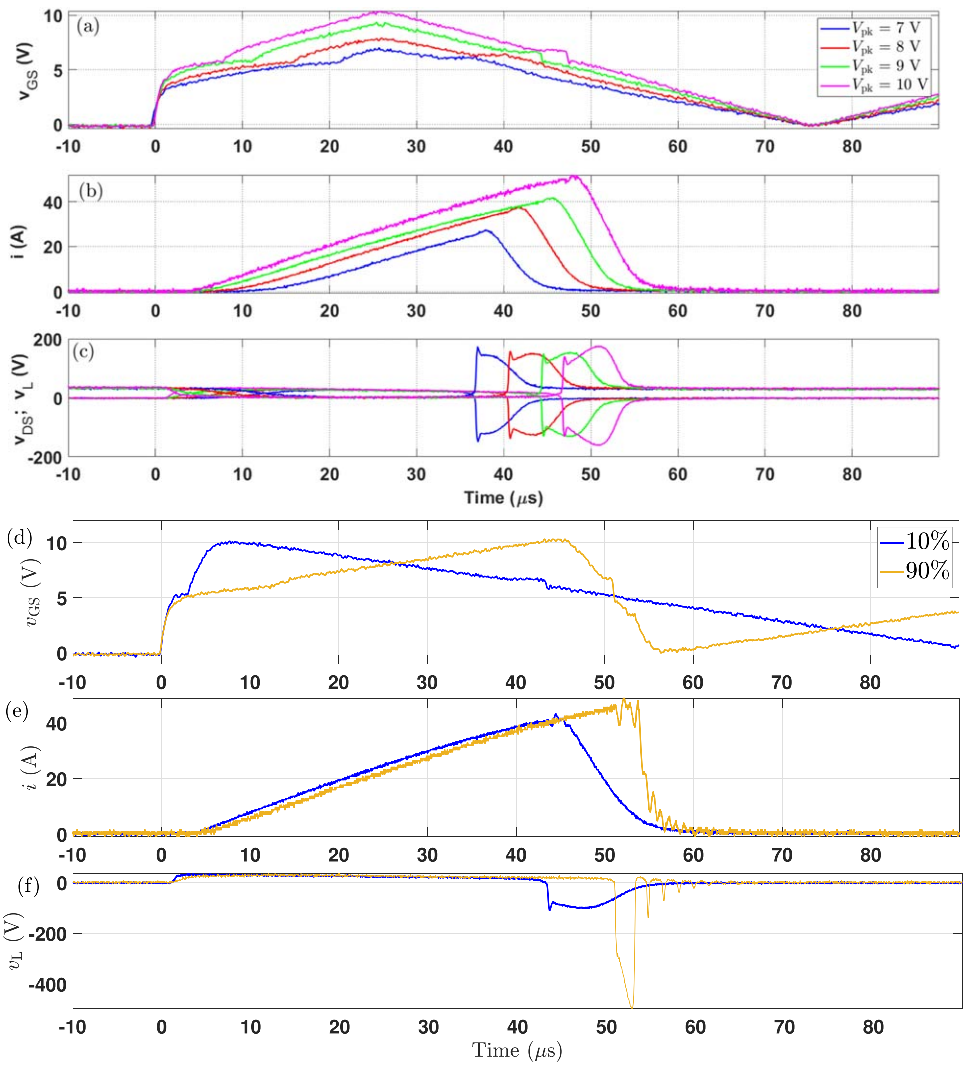

Figure 9. (a) Peak gate voltage is stepped from 7 V to 10 V; (b) TMS coil current pulse for respective gate voltage; (c) Drain-source voltage (above the zero reference) and TMS coil voltage; (d) 10% and 90% symmetry gate voltage; (e) TMS coil current pulse for respective gate voltage; (f) TMS coil voltage.

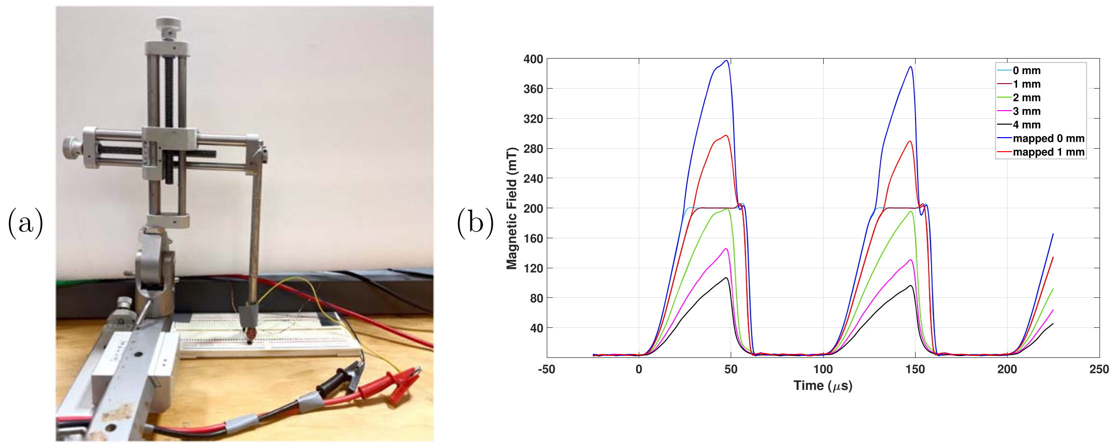

Figure 10. Laboratory setup for B-field measurement featuring an SS496A1 Hall effect sensor and a TMS coil mounted on an adjustable stand with vernier scale; (b)Experimental trials were conducted using an 80% symmetric triangular gate voltage with a 1 V SC input, measuring the magnetic field generated by the TMS coil at distances ranging from 0 mm to 4 mm from the sensor.

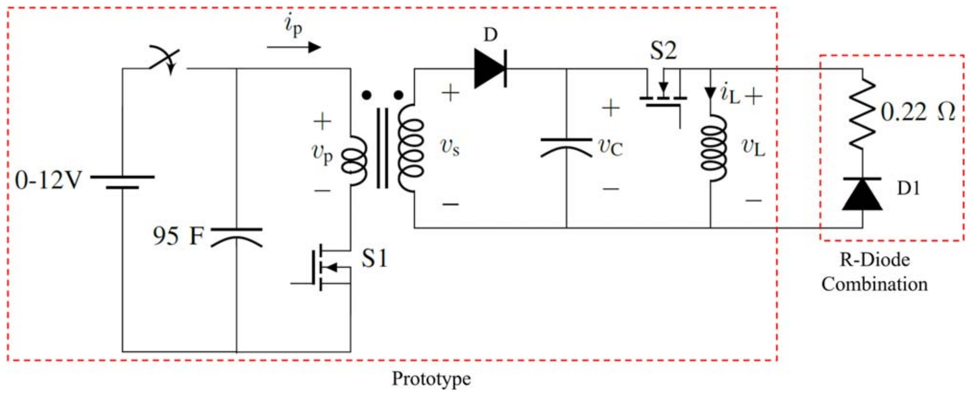

Figure 11. Circuit modification involves adding an R-diode combination in parallel to the existing prototype. For simplicity, only the main circuit of the prototype is illustrated, omitting the gate driver circuits for S1 and S2.

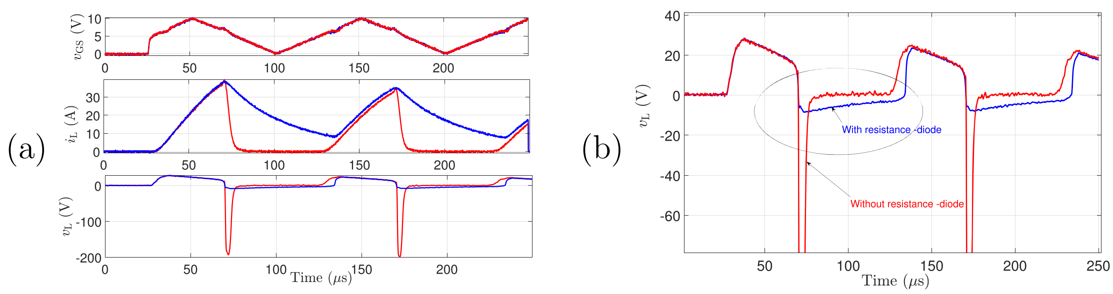

Figure 12. (a) Voltage Pulse TMS comparison between RLC prototype and enhanced version with resistor-diode combination (b) The zoomed-in view of the negative phase is presented, comparing the waveform with and without the resistor-diode combination.

discharge. This controlled discharge extends the duration of the negative phase of the voltage waveform across the TMS coil, allowing you to shape the pulse more effectively.

Figure 12 clearly shows the difference between the original prototype (figure 4) and the modification with the resistor-diode combination (figure 11). When the MOSFET S2 turns off, the current drop is delayed, allowing for more gradual energy dissipation. This delay in current reduction translates into a longer-lasting and more controllable negative phase of the TMS pulse.

7. Discussion

We have presented a new design approach for a supercapacitor-based pulse generator providing a test-bed for a low-cost flexible pulse generator for applications such as TMS excitation. This system can generate a tension of several hundred volts across the TMS coil using a low-voltage supercapacitor bank, and allows wave-shaping adjustment of the TMS current and voltage pulse, by varying the rise-fall symmetry of the triangular gate voltage. All experiments were conducted using a 1 V input from the supercapacitor (SC) during the initial testing phase of the prototype (figure 4). With this low input voltage, the design achieved a peak output voltage pulse of 500 V and generated a magnetic field exceeding 200 mT for a pulse of 100 μs width. These initial experiments served as a proof of concept, demonstrating the design's effectiveness and confirming its suitability for TMS applications, meeting the necessary requirements for successful stimulation. Using a supercapacitor bank with a 12 V input allows for the generation of multiple TMS pulses without the need to recharge the energy source. Due to the very low equivalent series resistance (ESR) of the supercapacitors, the voltage drop is minimal, enabling the voltage to be maintained across several pulse sequences, making it well-suited for reliable TMS applications. In the initial stage, with a 1 V input, we are generating 20 pulses per discharge. However, if there is a need to increase the number of pulses, we can replace the supercapacitor with one that has a higher capacitance value and charge it to a higher voltage (like 12 V). This modification would allow the circuit to continuously generate pulses in the range of 2000 pulses. The pulse count, however, is also dependent on the pulse width; a wider pulse width would reduce the total number of pulses.

An Arduino was chosen for this prototype design because it is easy to program and offers great flexibility in controlling various components. It is ideal for rapid development and experimentation, allowing us to send control signals to the S1 gate and manage the triangle waveform generator for S2, as shown in figure 4. The key advantage of using a programmable processor like the Arduino than any electronic circuit is its precise control, adaptability for future changes, and the convenience of integrating multiple functions into a single unit, making it a cost-effective and efficient solution for the prototype stage. While the Arduino is a suitable choice for this development, the possibility of using other micro-controllers/software will also be explored in the future.

Our prototype demonstrates that a supercapacitor (SC) can serve as a reliable and low-cost energy source for a TMS pulse generator, effectively replacing the high-voltage sources used in existing topologies (Peterchev *et al* 2011; Goetz *et al* 2012). By treating the MOSFET as more than just a switch, and using a triangular pulse, we observed that the TMS voltage and current pulse parameters could be controlled through adjustments in the rise and fall times of the triangular pulse. This approach confirms the SC's suitability as an alternative energy source and the enhanced functionality of the MOSFET in pulse shaping.

The pulses presented in this study are of smaller pulsewidth. This serves as a preliminary test to evaluate the suitability of the design for TMS applications. Higher power applications can be achieved with the same prototype, although this would necessitate additional safety measures, such as sealing the components to prevent accidental contact.

8. Conclusion

This article presents a new design technique for TMS pulse generator based on a small supercapacitor bank as the primary energy source, eliminating a high voltage DC power supply. We use medium-canister size supercapacitors with common low-cost passive components such as a step-up transformer based on an inexpensive core, medium voltage electrolytic capacitors and low-cost MOSFETs. The SC has proven to be an excellent energy source, capable of retaining its voltage across many pulse sequences without needing to be recharged. Additionally, in this approach, the MOSFET is treated as a dynamic element, enabling effective pulse shaping. Pulse shaping is an under-explored area in TMS, and by adjusting the symmetry of the triangular gate voltage, the pulse width can be varied, offering control over TMS pulse. The circuit prototype has the ability to adjust the pulse parameters which adds an innovative dimension previously under-explored in TMS pulse generators.

Acknowledgments

Soniya Raju gratefully acknowledges the University of Waikato Doctoral Scholarship for research support.

Data availability statement

All data that support the findings of this study are included within the article (and any supplementary files).

ORCID iDs

Soniya Raju https://orcid.org/0009-0001-1619-6736
Marcus Wilson https://orcid.org/0000-0001-6214-7727

References

Ali K, Wendt K, Sorkhabi M M, Benjaber M, Denison T and Rogers D J 2023 xtms: A pulse generator for exploring transcranial magnetic stimulation therapies *2023 IEEE Applied Power Electronics Conference and Exposition (APEC)* 1875–80

Barker A T, Garnham C W and Freeston I L 1991 Magnetic nerve stimulation: the effect of waveform on efficiency, determination of neural membrane time constants and the measurement of stimulator output *Electroencephalogr Clin. Neurophysiol. Suppl.* **43** 227–37

Barker A T, Jalinous R and Freeston I L 1985 Non-invasive magnetic stimulation of human motor cortex *The Lancet* **325** 1106–7

Camera F, Colantoni E, Casciati A, Tanno B, Mencarelli L, Di Lorenzo F, Bonnì S, Koch G and Merla C 2024 Dosimetry for repetitive transcranial magnetic stimulation: a translational study from alzheimers disease patients to controlled in vitro investigations *Phys. Med. Biol.* **69** 185001

Cheng L, Chen Z, Wang H, Guo F, Wu G, Xie L, Xiao J, Wang Y, Shen S and Ding W 2021 A novel avalanche transistor-based nanosecond pulse generator with a wide working range and high reliability *IEEE Trans. Instrum. Meas.* **70** 1–14

Cheng L, Mei K, Chen Z, Jia W, Wang Y, Wang H, Xie L, Shen S and Ding W 2022 High-voltage repetitive nanosecond pulse generator utilizing power synthesis of modified avalanche transistorized marx circuits *IEEE Trans. Instrum. Meas.* **71** 1–16

Eilers P H 2003 A perfect smoother *Anal. Chem.* **75** 3631–6

Elgenedy M A, Massoud A M, Holliday D, Ahmed S and Williams B 2017 Low-voltage dc input, high-voltage pulse generator using nano-crystalline transformer and sequentially charged mmc sub-modules, for water treatment applications *2017 IEEE Energy Conversion Congress and Exposition (ECCE)* 2144–9

Elserougi A, Ahmed S and Massoud A 2016 A boost converter-based ringing circuit with high-voltage gain for unipolar pulse generation *IEEE Trans. Dielectr. Electr. Insul.* **23** 2088–94

George M S *et al* 2010 Daily left prefrontal transcranial magnetic stimulation therapy for major depressive disorder: a sham-controlled randomized trial *Archives of General Psychiatry* **67** 507–16

Goetz S M, Pfaeffl M, Huber J, Singer M, Marquardt R and Weyh T 2012 Circuit topology and control principle for a first magnetic stimulator with fully controllable waveform *2012 Annual International Conference of the IEEE Engineering in Medicine and Biology Society* (IEEE) 4700–3

Gomez-Tames J, Laakso I and Hirata A 2020 Review on biophysical modelling and simulation studies for transcranial magnetic stimulation *Phys. Med. Biol.* **65** 24TR03

Iglesias A H 2020 Transcranial magnetic stimulation as treatment in multiple neurologic conditions *Curr. Neurol. Neurosci. Rep.* **20** 1–9

Jiang S, Zhang W, Wang Y, Li Z and Rao J 2022 A solid-state pulse adder for high-voltage short pulses and low-voltage long pulses *IEEE Trans. Plasma Sci.* **50** 3107–12

Khokhar F A, Voss L J, Steyn-Ross D A and Wilson M T 2021 Design and demonstration in vitro of a mouse-specific transcranial magnetic stimulation coil *IEEE Trans. Magn.* **57** 1–11

Koponen L M and Peterchev A V 2020 Transcranial magnetic stimulation: principles and applications *Neural Eng.* ed B He (Springer) 245–70

Kularatna N and Gunawardane K 2021 *Energy Storage Devices for Renewable Energy-Based Systems: Rechargeable Batteries and Supercapacitors* (Academic)

Kularatna N and Jayananda D 2020 Supercapacitor-based long time-constant circuits: A unique design opportunity for new power electronic circuit topologies *IEEE Industrial Electronics Magazine* **14** 40–56

Li L, Ning M, Dehuai C, Lun L, Qiang K, Mingjia L, Yong C and Yuan P 2015 Study on double resonant performance of air-core spiral tesla transformer applied in repetitive pulsed operation *IEEE Trans. Dielectr. Electr. Insul.* **22** 1916–22

Mankowski J and Kristiansen M 2000 A review of short pulse generator technology *IEEE Trans. Plasma Sci.* **28** 102–8

Menzies L, Chamberlain S R, Laird A R, Thelen S M, Sahakian B J and Bullmore E T 2008 Integrating evidence from neuroimaging and neuropsychological studies of obsessive-compulsive disorder: the orbitofronto-striatal model revisited *Neuroscience & Biobehavioral Reviews* **32** 525–49

Nieminen J O, Pospelov A S, Koponen L M, Yrjölä P, Shulga A, Khirug S and Rivera C 2022 Transcranial magnetic stimulation set-up for small animals *Frontiers in Neuroscience* **16** 935268

Osuch E A, Benson B E, Luckenbaugh D A, Geraci M, Post R M and McCann U 2009 Repetitive tms combined with exposure therapy for ptsd: a preliminary study *Journal of Anxiety Disorders* **23** 54–9

Peterchev A V, Deng Z-D and Goetz S M 2015 Advances in transcranial magnetic stimulation technology *Brain Stimulation: Methodologies and Interventions* ed I M Reti (Wiley) 10 165–89

Peterchev A V, Jalinous R and Lisanby S H 2007 A transcranial magnetic stimulator inducing near-rectangular pulses with controllable pulse width (cTMS) *IEEE Trans. Biomed. Eng.* **55** 257–66

Peterchev A V and Murphy D L 2013 Controllable pulse parameter transcranial magnetic stimulator with enhanced pulse shaping, in '2013 *6th International IEEE/EMBS Conference on Neural Engineering (NER)* (IEEE) 121–4

Peterchev A V, Murphy D L and Lisanby S H 2011 Repetitive transcranial magnetic stimulator with controllable pulse parameters *J. Neural Eng.* **8** 036016

Raju S, Kularatna N and Wilson M 2023 Supercapacitor based adjustable high power pulse generator for medical research applications *IECON 2023-49th Annual Conference of the IEEE Industrial Electronics Society* (IEEE) 1–6

Selvaraj J, Rastogi P, Prabhu Gaunkar N, Hadimani R L and Mina M 2018 Transcranial magnetic stimulation: Design of a stimulator and a focused coil for the application of small animals *IEEE Trans. Magn.* **54** 1–5

Smith M-C and Stinear C M 2016 Transcranial magnetic stimulation (TMS) in stroke: ready for clinical practice? *Journal of Clinical Neuroscience* **31** 10–4

Somaa F A, de Graaf T A and Sack A T 2022 Transcranial magnetic stimulation in the treatment of neurological diseases *Frontiers Neurol.* **13** 793253

Sorkhabi M M, Benjaber M, Wendt K, West T O, Rogers D J and Denison T 2021 Programmable transcranial magnetic stimulation: A modulation approach for the generation of controllable magnetic stimuli *IEEE Trans. Biomed. Eng.* **68** 1847–58

Tang A D *et al* 2018 Low intensity repetitive transcranial magnetic stimulation modulates skilled motor learning in adult mice *Scientific Reports* **8** 4016

Tang A D *et al* 2016 Construction and evaluation of rodent-specific rTMS coils *Frontiers in Neural Circuits* **10** 47

Tang A D, Makowiecki K, Bartlett C and Rodger J 2015 Low intensity repetitive transcranial magnetic stimulation does not induce cell survival or regeneration in a mouse optic nerve crush model *PloS One* **10** e0126949

Tang A, Thickbroom G and Rodger J 2017 Repetitive transcranial magnetic stimulation of the brain: mechanisms from animal and experimental models *The Neuroscientist* **23** 82–94

Udayanga S T S, Kokuhennadige S, Fernando J, Kularatna N and Steyn-Ross D A 2021 Supercapacitor assisted surge absorber (SCASA) technique: Selection of magnetic components based on permeance *2021 IEEE Applied Power Electronics Conference and Exposition (APEC)* (IEEE) 2299–304

Valchev V C and Van den Bossche A 2018 *Inductors and Transformers for Power Electronics* (CRC press)

Van Rooij S J, Arulpragasam A R, McDonald W M and Philip N S 2024 Accelerated tms-moving quickly into the future of depression treatment *Neuropsychopharmacology* **49** 128–37

Wassermann E M and Zimmermann T 2012 Transcranial magnetic brain stimulation: therapeutic promises and scientific gaps *Pharmacology & Therapeutics* **133** 98–107

Weinert H L 2007 Efficient computation for Whittaker-Henderson smoothing *Computational Statistics & Data Analysis* **52** 959–74

Wilson M T, Fulcher B D, Fung P K, Robinson P A, Fornito A and Rogasch N C 2018 Biophysical modeling of neural plasticity induced by transcranial magnetic stimulation *Clin. Neurophysiol.* **129** 1230–41

Wilson M, Tang A, Iyer K, McKee H, Waas J and Rodger J 2018 The challenges of producing effective small coils for transcranial magnetic stimulation of mice *Biomed. Phys. Eng. Express* **4** 037002

Yan J, Shen S and Ding W 2020 High-power nanosecond pulse generators with improved reliability by adopting auxiliary triggering topology *IEEE Trans. Power Electron.* **35** 1353–64

Zan X, Torres D R, Kheirollahi R, Lu X, Zheng S, Lu F and Avestruz A-T 2023 Medium voltage pulse power generator for accurate current interruption *IEEE Trans. Ind. Electron.* **70** 3604–15

Zhao Y, Xie W, Jiang J, Chen L, Feng S, Wang M and Wang Z 2019 Replacement of marx generator by tesla transformer for pulsed power system reliability improvement *IEEE Trans. Plasma Sci.* **47** 574–80